PASJ: Publ. Astron. Soc. Japan **47**, 265–272 (2008)

arXiv:astro-ph/0103031v1 2 Mar 2001

The Radio and Gamma-Ray Luminosities of Blazars

L. Zhang,[1,2] K.S. Cheng,[2] J.H. Fan[3]

[1] *Department of Physics, Yunnan University, Kunming, P.R. China*
[2] *Department of Physics, the University of Hong Kong, Hong Kong, P.R. China*
[3] *Center for Astrophysics, Guangzhou University, Guangzhou, 510400, P.R. China*

(Received 1995 February 22; accepted 1995 April 6)

Abstract

Based on the γ-ray data of blazars in the third EGRET catalog and radio data at 5 GHz, we studied the correlation between the radio and γ-ray luminosities using two statistical methods. The first method was the partial correlation analysis method, which indicates that there exist correlations between the radio and γ-ray luminosities in both high and low states as well as in the average case. The second method involved a comparison of expected γ-ray luminosity distribution with the observed data using the Kolmogorov–Smirnov (KS) test. In the second method, we assumed that there is a correlation between the radio and γ-ray luminosities and that the γ-ray luminosity function is proportional to the radio luminosity function. The KS test indicates that the expected gamma-ray luminosity distributions are consistent with the observed data in a reasonable parameter range. Finally, we used different γ-ray luminosity functions to estimate the possible 'observed' γ-ray luminosity distributions by GLAST.

Key words: galaxies: active — quasars: general — gamma rays

1. Introduction

Although the correlation between the radio and γ-ray luminosities of blazars has been widely studied, two opposite conclusions have been made. Based on the data observed by EGRET at different observation times, a moderate correlation between the radio and γ-ray luminosities has been obtained (e.g. Stecker et al. 1993; Padovani et al. 1993; Salamon, Stecker 1994; Dondi, Ghisellini, 1995; Stecker, Salmon , 1996; Mücke et al. 1997; Mattox et al. 1997; Zhou et al. 1997; Fan et al. 1998; Cheng et al. 2000). However, Mücke et al. (1997) performed Monte Carlo simulations of selected data sets and applied different correlation techniques in view of a truncation bias caused by sensitivity limits of the surveys. In their analysis, they used radio and γ-ray luminosity functions given by Dunlop and Peacock (1990) and Chiang et al. (1995). After a careful analysis, they claimed that there is no correlation between the radio and γ-ray luminosities for simultaneously observed radio and γ-ray data.

Many models have been proposed to explain the origin of the blazar γ-ray emission, including synchrotron self-Compton (e.g. Maraschi et al 1992), inverse Compton scattering on photons produced by an accretion disk (e.g. Dermer et al. 1992; Zhang, Cheng 1997), or scattered by ambient material, or reprocessed by broad-line clouds (e.g. Sikora et al. 1994; Blandford, Levinson 1995; Xie et al. 1997), synchrotron emission by ultra-relativistic electrons and positrons (e.g, Ghisellini et al. 1993; Cheng et al. 1993), and electromagnetic cascade by collision of ultra-relativistic nucleons (e.g, Mannheim, Biermann 1992; Mannheim 1993; Cheng, Ding 1994). However, there is no consensus yet on the dominant emission process.

Correlation analye between different wavebands are important for us to understand the γ-ray emission from blazars. For example, if radio emission is produced by high-energy electrons in the jet via synchrotron radiation, it is likely that these electrons contribute part of the γ-rays due to inverse Compton scattering. In this sense, it seems reasonable to expect some correlation between the radio and γ-ray luminosities. Here, we revisit the correlation between the radio and γ-ray luminosities of blazars using the observed γ-ray data in the third catalog of EGRET (Hartman et al. 1999) and radio data at 5 GHz (see table 1), since the data in these two bands are presently complete. In section 2, we list the observed data and discuss a correlation analysis based on the use of a partial correlation analysis. Further, we estimate γ-ray luminosity distribution of the observed blazars at 100 MeV and compared it with the observed data in section 3. Finally, we give our conclusions and a brief discussion in section 4.

Throughout the paper we use a Hubble constant, H_0, of 75 km s^{-1} Mpc^{-1} and the deceleration parameter, q_0, of 0.5.

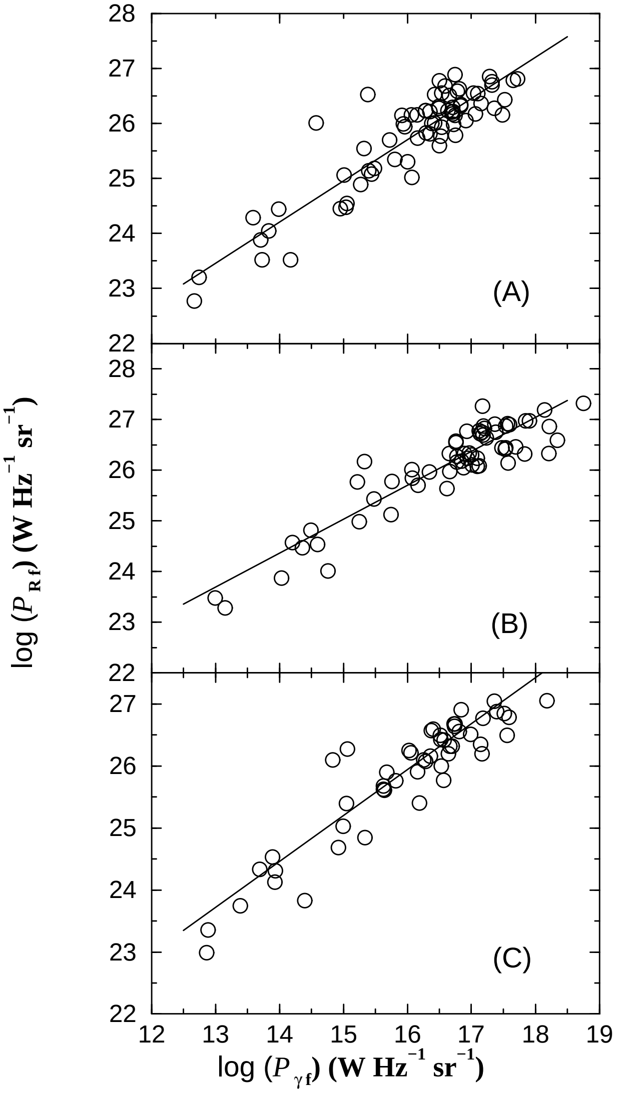

Fig. 1.. Correlations of the γ-ray luminosity with radio luminosity. (A) low state. (B) high state. (C) average case. The differential luminosity is used in a specific frequencies ν, where ν is 5 GHz for the radio and 100 MeV for the γ-rays.

2. Observed Data and Correlation Analysis

The third EGRET catalog includes 66 positive and 25 marginal detections of γ-ray loud blazars above 100 MeV (Hartman et al. 1999). We list 67 of the identified blazars (including Markarian 501) and 25 marginal blazars in table 1. For each source, its γ-ray fluxes above 100 MeV in both the high and low states are the maximum and minimum observed data in the third EGRET catalog. The average γ-ray flux is the value labeled by P1234 in the third catalog. For radio data at 5 GHz, part of our sample were taken from those in both high and low states compiled by Cheng et al. (2000). The average radio data at 5 GHz were taken from a database provided by the University of Michigan Radio Astronomy Observatory.

From table 1, we can obtain that the mean value of the redshifts in our sample is 0.96 ± 0.06 and the average value of integrated spectral index of γ-rays is 1.22 ± 0.01 using a weighted average method. In order to analyze the correlation between the radio and γ-ray luminosities, we made a K-correction for the observed fluxes listed in table 1 by using

$$F(\nu) = F_{\rm obs}(\nu)(1+z)^{\alpha-1} \quad , \tag{1}$$

where z is the redshift and α is the spectral index at the frequency ν. We used $\alpha = 0$ in the radio band and $\alpha = 1.22$ in the γ energy range when the spectral indices of the sources were not known. When the redshift was not known, we used the mean value of our sample, i.e. $z = 0.96$. We now consider the differential luminosity, which is given by

$$P_i(E_i) = P_{i\rm f}\left(\frac{E_i}{E_{i\rm f}}\right)^{-\alpha_i} \quad , \tag{2}$$

where α_i is the spectral index, i = R is for radio and $i = \gamma$ for γ-rays. We chose $E_{\gamma\rm f}$ = 100 MeV. If the flux density at a certain energy and the spectral index are known, the differential luminosity per unit solid angle is given by $P_{i\rm f} = S_i(E_{i\rm f})[R_0^2 r^2 (1+z)^2]$, where S_i is the radio flux density for i = R or γ-ray flux density for $i = \gamma$, z is the redshift, r is the co-moving coordinate of the source, R_0 is the present cosmological scale factor, and $R_0 r = (2c/H_0)[1-(1+z)^{-1/2}]$. Therefore, for radio data,

$$\begin{aligned} P_{\rm Rf} = & \quad 10^{-30}\left(\tfrac{2c}{H_0}\right)^2 [1-(1+z)^{-1/2}]^2 \\ & (1+z)^{\alpha_{\rm R}+1} S_{\rm R\ obs}(E_{\rm Rf}) \quad {\rm W\ Hz^{-1}\ sr^{-1}} \quad , \end{aligned} \tag{3}$$

where $S_{\rm R\ obs}(E_{\rm Rf})$ is in units of Jy. For γ-ray data,

$$\begin{aligned} P_{\gamma\rm f} & \approx 6.6 \times 10^{-41}\left(\tfrac{2c}{H_0}\right)^2 [1-(1+z)^{-1/2}]^2 \alpha_\gamma \\ & (1+z)^{\alpha_\gamma+1} F_{\rm obs}(> 100\ {\rm MeV}) \quad {\rm W\ Hz^{-1}\ sr^{-1}} \ , \end{aligned} \tag{4}$$

where $F_{\rm obs}(>$ 100MeV) is the integrated γ-ray flux above 100 MeV in units of 10^{-7} cm^{-2} s^{-1} observed by EGRET and $\alpha_\gamma + 1$ is differential spectral index.

Using the observed data in table 1 and equationsq (4) and (5), we obtained the differential luminosities at 5 GHz and 100 MeV. We could thus consider the correlation between the radio and γ-ray luminosities in both the high and low states and for the average case. In the low state, the correlation between luminosities gives

$$\log_{10}{\rm P_{Rf}} = (13.7 \pm 0.7) + (0.75 \pm 0.04)\log_{10}{\rm P_{\gamma f}} \quad .(5)$$

In the high sate, we have

$$\log_{10}{\rm P_{Rf}} = (15.0 \pm 0.7) + (0.67 \pm 0.04)\log_{10}{\rm P_{\gamma f}} \quad .(6)$$

For the average case, we have

$$\log_{10}{\rm P_{Rf}} = (14.1 \pm 0.7) + (0.74 \pm 0.04)\log_{10}{\rm P_{\gamma f}} \quad .(7)$$

Table 1. Blazar sample*.

Source^a	z	S_R^h (Jy)	S_R^l (Jy)	S_R^{av}(Jy)^b	F_γ^h	F_γ^l	F_γ^{av}	α_γ
0202+149	1.202	3.68± 0.04	1.56± 0.11	2.91± 0.05	5.28± 2.64	2.36± 0.56	0.87± 0.28	1.23±0.15
0208-512	1.003		3.31± 0.12		13.41± 2.49	3.50± 1.10	8.55± 0.45	0.99±0.02
0219+428	0.444	2.55± 0.03	0.52± 0.04	2.05± 0.04	2.53± 0.58	1.21± 0.39	1.87± 0.29	1.01±0.07
0235+164	0.940	4.23± 0.02	0.23± 0.05	1.62± 0.06	6.51± 0.88	1.16± 0.40	2.59± 0.37	0.85±0.06
0336-019	0.852	2.29± 0.11	1.18± 0.08	2.39± 0.03	17.76± 3.66	1.31± 0.76	1.51± 0.35	0.84±0.11
0420-014	0.915	6.99	2.03± 0.11	3.17± 0.04	6.42± 3.42	0.93± 0.47	1.63± 0.31	1.44±0.11
0440-003	0.844	1.67± 0.08	1.18± 0.02	1.62± 0.07	8.59± 1.20	2.23± 0.41	1.25± 0.26	1.37±0.10
0446+112	1.207	1.89± 0.02	0.50± 0.03	1.55± 0.07	10.90± 1.94	0.63± 0.33	1.49± 0.25	1.27±0.09
0454-234	1.009	2.15± 0.07	1.49± 0.08		1.47± 0.42	0.81± 0.26	0.81± 0.26	2.14±0.32
0454-463	0.858	1.90± 0.09	1.90± 0.09		2.28± 0.74	0.55± 0.26	0.77± 0.21	1.75±0.22
0458-020	2.286	4.05± 0.06	1.90± 0.05	2.94± 0.07	6.82± 4.13	0.95± 0.32	1.12± 0.23	1.45±0.16
0528+134	2.070	6.38± 0.10	1.99± 0.04	3.46± 0.09	35.10± 3.68	3.24± 1.43	9.35± 0.36	1.46±0.02
0537-441	0.896	5.30± 0.01	2.52± 0.02		9.11± 1.46	1.65± 0.45	2.53± 0.31	1.41±0.07
0716+714	0.300	1.17± 0.02	0.31± 0.05	0.62± 0.02	4.57± 1.11	0.93± 0.47	1.78± 0.20	1.19±0.06
0735+178	0.424	4.82± 0.17	1.03± 0.03	2.69± 0.08	2.93± 0.99	1.58± 0.42	1.64± 0.33	1.60±0.17
0827+243	2.050	0.67	0.59± 0.01	0.97± 0.09	11.10± 6.01	1.56± 0.59	2.49± 0.39	1.42±0.12
0829+046	0.180	2.27± 0.20	0.66± 0.18	1.14± 0.03	3.35± 1.63	1.68± 0.51	1.57± 0.48	1.47±0.24
0836+710	2.172	2.70± 0.07	1.65± 0.09	2.13± 0.01	3.34± 0.90	0.86± 0.20	1.02± 0.47	1.62±0.10
0851+202	0.306	5.01± 0.08	0.99± 0.09	2.10± 0.04	1.58± 0.69	0.97± 0.44	1.06± 0.30	1.03±0.18
0954+556	0.901	2.29± 0.11	1.71± 0.20	1.98± 0.01	4.72± 1.55	0.65± 0.25	0.91± 0.16	1.12±0.10
0954+658	0.368	1.62± 0.03	0.18± 0.03	0.64± 0.03	1.80± 0.94	0.66± 0.17	0.60± 0.15	1.08±0.12
1101+384	0.031	1.42± 0.11	0.43± 0.04	0.72± 0.01	2.71± 0.69	0.90± 0.36	1.39± 0.18	0.57±0.05
1156+295	0.729	2.22± 0.04	0.88± 0.02	1.40± 0.03	16.30± 4.00	0.83± 0.20	0.75± 0.18	0.98±0.11
1219+285	0.102	2.39± 0.07	0.54± 0.03	0.94± 0.02	5.36± 1.41	0.69± 0.26	1.15± 0.78	0.73±0.08
1222+216	0.435	2.23± 0.07	1.57± 0.10	1.88± 0.04	4.81± 1.53	0.69± 0.29	1.39± 0.18	1.28±0.07
1226+023	0.158	44.56± 0.38	30.73± 0.89	37.56± 0.22	4.83± 1.18	0.85± 0.42	1.54± 0.12	1.58±0.06
1229-021	1.045	1.04± 0.03	0.94± 0.03	0.94± 0.03	1.55± 0.41	0.49± 0.21	0.69± 0.15	1.85±0.19
1253-055	0.538	17.82± 0.12	10.13± 0.29	11.27± 0.09	26.70± 1.07	0.76± 0.36	7.42± 0.28	0.96±0.02
1331+170	2.084		0.70		3.31± 1.93	0.94± 0.27	0.44± 0.16	1.41±0.27
1406-076	1.494	1.08± 0.04	0.73± 0.04	0.81± 0.02	12.84± 2.34	1.04± 0.39	2.74± 0.22	1.29±0.06
1424-418	1.522	4.08± 0.14	2.18± 0.09		5.53± 1.63	1.53± 0.86	1.19± 0.27	1.13±0.11
1510-089	0.361	4.33± 0.04	0.96± 0.14	2.53± 0.04	4.94± 1.83	1.26± 0.53	1.80± 0.38	1.47±0.12
1604+159	0.357		0.50		4.20± 1.23	1.23± 0.47	1.28± 0.41	1.06±0.21
1606+106	1.227	1.98± 0.09	1.07± 0.20	1.62± 0.02	6.24± 1.30	2.10± 0.92	2.50± 0.45	1.63±0.15
1611+343	1.404	4.49± 0.03	2.07± 0.09	3.39± 0.05	6.89± 1.53	1.90± 0.40	2.65± 0.40	1.42±0.09
1622-253	0.786	2.34± 0.09	1.53± 0.03	1.94± 0.04	8.25± 3.50	1.01± 0.40	2.12± 0.35	1.07±0.04
1622-297	0.815	3.97± 0.14	2.07± 0.09	2.26± 0.04	32.10± 3.35	1.24± 0.36	4.75± 0.37	1.07±0.04
1633+382	1.814	3.52± 0.03	1.91± 0.02	2.30± 0.01	10.70± 0.96	3.18± 1.04	5.84± 0.52	1.15±0.05
1652+398	0.033	1.96± 0.07	1.04± 0.13	1.46± 0.01	3.20± 1.30	1.80± 0.50	2.50± 0.70	0.30±0.12
1730-130	0.902	9.01± 0.10	4.10± 0.05	5.81± 0.09	10.48± 3.47	1.81± 0.74	3.61± 0.34	1.23±0.06
1739+522	1.375	3.36± 0.03	0.58± 0.05	1.91± 0.06	4.49± 2.69	0.97± 0.47	1.82± 0.30	1.42±0.13
1741-038	1.054	4.90± 0.06	1.50± 0.09	2.88± 0.09	4.87± 1.96	1.76± 0.47	1.17± 0.33	1.42±0.25
1830-210	1.000		7.92		9.93± 2.48	1.78± 0.88	2.66± 0.37	1.59±0.08
1933-400	0.966	1.48± 0.08	0.66± 0.01		9.39± 3.14	1.40± 0.34	0.85± 0.27	1.86±0.26
2032+107	0.601	1.08± 0.04	0.26± 0.17	0.62± 0.02	3.59± 1.50	1.02± 0.38	1.33± 0.31	1.83±0.17
2052-474	1.489		2.52± 0.10		3.50± 2.09	1.13± 0.35	0.96± 0.32	1.04±0.18
2155-304	0.116	0.56± 0.07	0.18± 0.09	0.37± 0.02	3.04± 0.77	0.79± 0.35	1.32± 0.32	1.35±0.15
2200+420	0.069	9.98± 0.07	1.69± 0.05	3.10± 0.05	3.99± 1.16	0.88± 0.38	1.11± 0.31	1.60±0.17
2209+236	1.000	1.21± 0.16	0.60± 0.13		4.57± 2.05	1.23± 0.35	0.69± 0.23	1.48±0.30
2230+114	1.037	5.39± 0.14	3.44± 0.08	4.16± 0.12	5.16± 1.50	1.21± 0.35	1.92± 0.28	1.45±0.08
2251+158	0.859	24.00± 0.72	7.92± 0.14	10.67± 0.14	11.61± 1.84	2.46± 0.96	5.37± 0.40	1.21±0.03
2356+196	1.066	0.86± 0.08	0.59± 0.10	0.73± 0.05	2.63± 0.90	1.28± 0.55	0.83± 0.28	1.09±0.18
0414-189*	1.536		1.35± 0.08		4.95± 1.61	1.37± 0.77	0.91	2.25±0.47
0430+2859*					7.58± 2.21	1.60± 0.33	2.20± 0.28	0.90±0.05

Table 1. Continued

Source^a	z	S_R^h (Jy)	S_R^l (Jy)	S_R^{av}(Jy)^b	F_γ^h	F_γ^l	F_γ^{av}	α_γ
0459+060*	1.106				3.40± 1.82	1.19± 0.32	0.61± 0.21	1.36±0.23
0616-116*					4.79± 1.63	1.49± 0.82	1.09± 0.34	1.67±0.27
0738+5451*	0.723				4.21± 0.83	1.14± 0.63	1.11± 0.24	1.03±0.10
0850-1213*	0.566				4.44± 1.16	1.40± 0.44		0.58±0.21
1243-072*	1.286		1.14± 0.04		4.41± 2.96	0.60± 0.25	0.98± 0.21	1.73±0.11
1334-127*	0.539				2.02± 1.16	1.14± 0.38	0.55± 0.19	1.62±0.26
1725+044*	0.296		1.25± 0.04		3.02± 1.88	1.33± 0.61	1.79± 0.41	1.67±0.16
1759-396*				2.29± 0.06	14.57± 4.89	1.75± 0.47	0.98± 0.29	2.10±0.24
1908-201*		2.37± 0.03	2.10± 0.05	0.65± 0.03	3.71± 2.03	1.49± 0.34	1.75±0.27	1.39±0.10
1936-155*	1.657	1.69± 0.08	0.63± 0.03		5.50± 1.86	0.76± 0.30	0.74	2.45±0.90
2022-077*	1.388				7.45± 1.34	2.18± 0.38	2.12± 0.35	1.38±0.10
2320-035*	1.411				3.82± 1.01	0.82± 0.44	0.60	
2351-456*	1.992				4.28± 2.03	1.18± 0.52	1.43± 0.37	1.38±0.22
0234+285	1.213	4.87± 0.06	1.45± 0.04	2.64± 0.07	3.41± 1.16	1.09± 0.44	1.38± 0.26	1.53±0.13
0506-612	1.093	1.50± 0.08	1.50± 0.08		2.88± 1.15	0.64± 0.12	0.72± 0.17	1.40±0.15
0521-365	0.055	8.87± 0.17	6.52± 0.16	8.06± 0.04	3.19± 0.72	1.95± 0.44	1.58± 0.35	1.63±0.26
0804+499	1.433	1.94± 0.13	0.22± 0.04		1.51± 0.61	0.83± 0.39	1.07± 0.25	1.15±0.24
0917+449	2.180	2.34± 0.06	1.00± 0.02		3.35± 1.30	1.14± 0.33	1.38± 0.20	1.19±0.08
1127-145	1.187	5.62± 0.17	2.95± 0.10	3.63± 0.02	6.18± 1.80	1.08± 0.59	0.99± 0.24	1.70±0.20
1313-333	1.210	1.47± 0.03	1.21± 0.18		3.18± 1.90	1.62± 0.53	1.46± 0.25	1.28±0.11
0119+041*	0.637	2.07± 0.09	1.22± 0.06		2.03± 0.58	1.34± 0.43	0.51± 0.27	1.63±0.41
0130-171*	1.022		1.00± 0.07		1.38± 0.68	0.92± 0.52	1.16± 0.30	1.50±0.17
0415+379*	0.049	8.67± 0.19	5.81± 0.04	6.44± 0.09	6.02± 1.71	1.02± 0.31	1.28± 0.26	1.59±0.20
0537-286*	3.110	1.19± 0.10	1.02± 0.07	1.16± 0.08	3.50± 1.18	0.96± 0.49	0.69± 0.27	1.47±0.36
0539-057*	0.839		1.56± 0.08			6.65± 1.95	1.00	
0803+5126*	1.140				2.34± 1.37	0.99± 0.26	0.87± 0.24	1.76±0.22
1011+496*	0.200				0.80± 0.30	0.44± 0.24	0.48± 0.14	0.90±0.18
1055+567*	0.410				1.61± 1.01	0.65± 0.16	0.50± 0.14	1.51±0.28
1237+0459*				1.52± 0.86	0.62± 0.21	0.65± 0.15	1.48±0.27	
1324+224*	1.400	1.66± 0.17	1.29± 0.15	1.52± 0.07	6.84± 2.26	0.95± 0.27	0.52± 0.16	1.58±0.16
1504-166*	0.876	2.72± 0.07	2.12± 0.08	2.39± 0.03	3.32± 1.03	1.65± 0.63	0.88	
1514-241*	0.042	3.00± 0.05	1.35± 0.04	2.23± 0.08	3.72± 1.83	1.85± 0.61	0.84± 0.28	1.66±0.27
1716-771*					4.05± 2.31	1.54± 0.57	0.84± 0.40	1.74±0.24
1808-5011*					6.21± 1.97	0.73± 0.33	0.59± 0.27	1.93±0.28
2105+598*					3.32± 0.96	1.62± 0.76	1.98± 0.41	1.21±0.14
2206+650*					3.08± 1.32	1.86± 0.82	2.44± 0.55	1.29±0.15
2250+1926*					6.22± 2.15	1.06± 0.38	0.58± 0.28	1.36±0.35
2346+385*	1.032				3.75± 1.03	0.85± 0.36	0.61± 0.32	1.47±0.40

: γ-ray flux is in units of10^{-7} cm^{-2} s^{-1}

a: the data of source names which are unmarked by stars are taken from those compiled by Cheng et al. (1999), the radio data of the source name which are marked by stars in high state or low state are taken from Kühr et al. (1981).

b: the averaged radio data are taken from the database provided by the University of Michigan Radio Astronomy Observatory.

As pointed out by Padovani (1992), because our sample was flux-limited, the luminosity was strongly correlated with redshift, would result in a spurious correlation. Therefore, we used a partial correlation analysis in our analysis, i.e. we examined the correlations between the radio and γ-ray luminosities excluding the dependence on the redshift. The correlation coefficients used for the analysis were the Spearman Rank–Order correlation coefficients (Press et al. 1992). In the low state (72 sources), the partial correlation coefficient is $r \approx 0.26$ (with chance probability $P \approx 2.6 \times 10^{-2}$), which was derived by using the fact that the correlation coefficients between log $P_{\gamma\mathrm{f}}$ and log P_{Rf}, log $P_{\gamma\mathrm{f}}$ and log z, and log P_{Rf} and log z are 0.904, 0.972, and 0.903 respectively. In the high state (62 sources), the correlation coefficients between log $P_{\gamma\mathrm{f}}$ and log P_{Rf}, log $P_{\gamma\mathrm{f}}$ and log z, and log P_{Rf} and log z are 0.919, 0.967, and 0.919 respectively; the partial correlation coefficient is thus $r \approx 0.30$ (with chance probability $P \approx 1.8 \times 10^{-2}$). Therefore, we may conclude that there exist correlations between the radio and γ-ray luminosities in both the high and low states. For the average case, from table 1, there are 51 sources which have average observed radio data. The average γ-ray flux for each source is the value (labeled P1234) in the third EGRET catalog (Hartman et al. 1999). The partial correlation analysis gives $r \approx 0.28$ with a chance probability, P, of $\approx 3.9 \times 10^{-2}$, which is at least a marginal correlation. Figure 1. shows the correlation between the luminosities for the above three cases.

3. Gamma-Ray Luminosity Distribution

We now consider the γ-ray luminosity distribution in order to further discuss whether there is a correlation between the radio and γ-ray luminosities. Using a pre-existing radio luminosity function and assuming that the radio and γ-ray luminosity are related [the correlation coefficients are given by equations (6), (5) and (7)], we could calculate the γ-ray luminosity distributions in the low, high states, and average cases following the method given by Stecker et al. (1993). As a comparison, when we calculated the γ-ray luminosity distribution in the average case, we used γ-ray luminosity function given by Chiang and Mukherjee (1998). These expected distributions were compared to the observed distribution. In figure 2., the normalized cumulative observed γ-ray luminosity distributions in the low, high states, and the average case are shown (dotted curves).

If the γ-ray luminosity function (ρ_γ) is given, the total number of sources of the luminosity, $P_{\gamma\mathrm{f}}$, seen at Earth is (Salamon, Stecker 1994)

$$n_{\mathrm{obs}} d(\log_{10} P_{\gamma\mathrm{f}}) = \int_0^{R_0 r_{\max}} 4\pi R_0^3 r^2 \rho_\gamma(P_{\gamma\mathrm{f}}, z) dr \; d(\log_{10} P_{\gamma\mathrm{f}}) \quad , \tag{8}$$

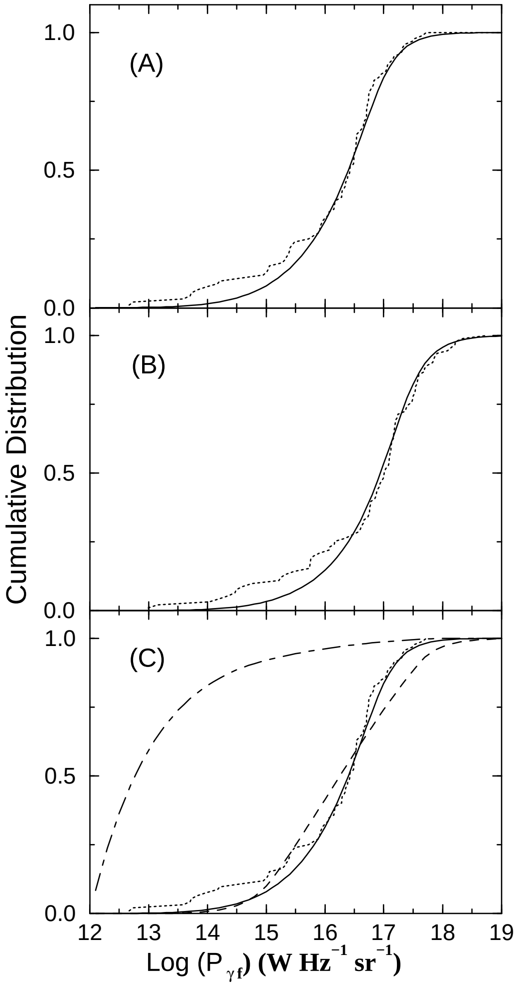

Fig. 2.. The Comparison of observed and expected cumulative distributions of the blazar γ-ray luminosities at 100 MeV. (A) low state. (B) high state. (C) average case. For the average case, the γ-ray luminosity distributions calculated by using Eqs. (12) and (14) are represented by solid, dashed ($\gamma_1 = 1.2$ and $\gamma_2 = 2.2$) and dot-dashed ($\gamma_1 = 2.9$ and $\gamma_2 = 2.6$) curves respectively. Dotted curves represent the observed distributions.

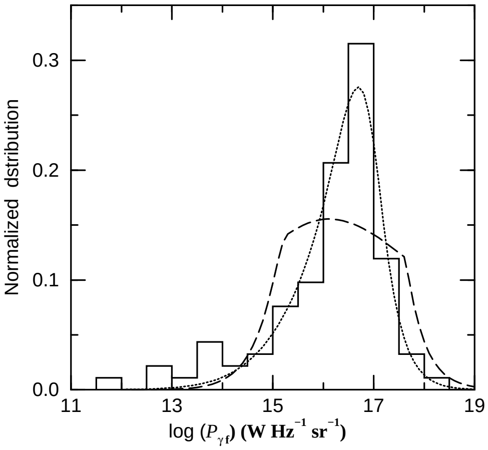

Fig. 3.. The comparison of the differential γ-ray luminosity distributions calculated by using Eqs. (12) (dotted curve) and (14) (dashed curve) with the observed data (histogram).

where $P_{\gamma\mathrm{f}}$ is given by equation (2) for a source with spectral index α_γ, and $R_0 r_{\max}$ is the maximum detectable distance which is found by using equation (5) and substituting the flux sensitivity, $F_{\gamma\mathrm{lim}}$, for F_{obs}. We can convert $R_0 r_{\max}$ to $z_{\max}$ using the relation of $R_0 r$ and z. In other words, the maximum redshift can be estimated by

$$(1+z_{\max})^{(\alpha_\gamma+1)}[(1+z_{\max})^{-1/2}-1]^2 = \qquad (9)$$
$$P_{\gamma\ \mathrm{f}}/[(2c/H_0)^2 S_{\gamma\ \mathrm{lim}}] \quad .$$

It should be noted that the co-moving density, ρ_γ, is in units of $\mathrm{Mpc}^{-3}\times$(unit interval of $\log_{10}P_\gamma)^{-1}$.

Salamon and Stecker (1994) assumed that (i) there is a linear relation between the γ-ray luminosity ($P_{\gamma\mathrm{f}}$) and the radio luminosity, i.e. $P_{\gamma\mathrm{f}} = 10^{\xi} P_{\mathrm{Rf}}$ and (ii) $\rho_\gamma = \eta\rho_{\mathrm{R}}$, where η is a normalization factor and ρ_{R} is a radio luminosity function. They found $\xi = -9.8$ by fitting 38 EGRET sources. Here, we assume that $P_{\mathrm{Rf}} = 10^{a} P^{b}_{\gamma\mathrm{f}}$, where the values of a and b in the high, low states, and for average case were estimated by equations (5), (6), and (7) respectively. The radio luminosity function is given by Dunlop and Peacock (1990)

$$\rho_{\mathrm{R}}(P_{\mathrm{R}}, z) \sim \left\{ \left[\frac{P_R}{P_c(z)}\right]^{0.83} + \left[\frac{P_R}{P_c(z)}\right]^{1.96} \right\}^{-1} \quad , (10)$$

where $\mathrm{Log}P_c(z) = 25.26 + 1.18z - 0.28z^2$, P_{R} is differential radio luminosity in units of W Hz^{-1} sr^{-1}, and ρ_{R} is co-moving density in units of $\mathrm{Mpc}^{-3}\times$(unit interval of $\log_{10}P_{\mathrm{R}})^{-1}$. Using above assumptions and equation (10), we have

$$n_{\mathrm{obs}} d(\log_{10}P_{\gamma\mathrm{f}}) = 2\pi\eta \left(\frac{2c}{H_0}\right)^3 \int_0^{z_{\max}} \qquad (11)$$
$$\frac{[(1+z)^{-1/2}-1]^2}{(1+z)^{5/2}} \rho_{\mathrm{R}}(10^a P^b_{\gamma\mathrm{f}}, z) dz\ d(\log_{10}P_{\gamma\mathrm{f}}) \quad ,$$

where $z_{\max}$ is determined by equation (10). Generally, once the $z_{\max}$ is given, we can obtain the γ-ray luminosity distribution. Because we assumed a maximum cutoff redshift of $z_{\max} = 5$, the upper limit of equation (12) is min ($z_{\max}$, 5). In order to estimate the γ-ray luminosity distribution using equation (12), we needed to know the γ-ray flux sensitivity and to then determine two parameters (a, b). We adjusted a and b within the allowed range, which is limited by equation (5) in the low state or by equation (6)in the high state. We used $a = 13.7$, $b = 0.76$, $F_{\gamma\ \mathrm{lim}}(>$ 100 MeV)$=0.5\times10^{-7}\mathrm{cm}^{-2}\ \mathrm{s}^{-1}$ in the low state, $a = 14.0$, $b = 0.68$, $F_{\gamma\ \mathrm{lim}}(>$ 100 MeV)$= 1.5\times10^{-7}$ cm^{-2} s^{-1} in the high state, and $a = 14.1$, $b = 0.74$ and $F_{\gamma\ \mathrm{lim}}(>$ 100 MeV)$= 0.5\times10^{-7}$ cm^{-2} s^{-1} for the average case. We used one sample KS test to compare the cumulative distributions with the observed ones. The maximum deviation are 0.09 in the low state (92 sources), 0.1 in the high state (91 sources) and 0.07 for the average case (92 sources). Therefore, the null hypothesis cannot be rejected at the $>$ 80% confidence level. Comparisons of the observed data and our results in the low, high states, and the average case are shown in panels (A), (B), and (C) of figure 2., respectively.

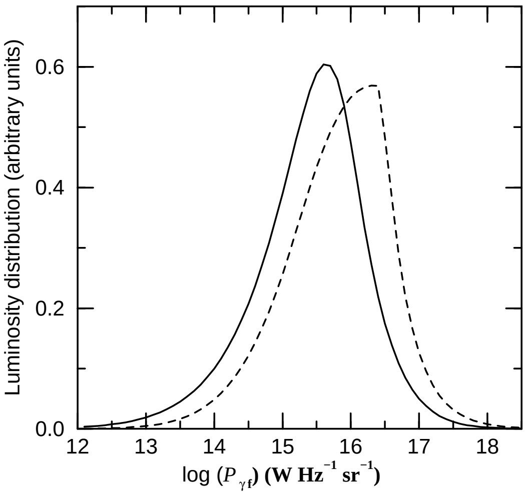

Fig. 4.. The expected differential distributions of average γ-ray luminosities of the blazars at 100 MeV. The threshold of GLAST is used ($F_{\gamma\ lim}(>100$ MeV$) = 3\times10^{-9}$ cm^{-2} s^{-1}). The γ-ray luminosity distributions calculated by using Eq. (12) and Eq. (14) are represented by solid and dashed curves respectively.

For a comparison, in the average case, we could also estimate the average γ-ray luminosity distribution using the γ-ray luminosity function of the EGRET blazars. The γ-ray luminosity function can be expressed as (Chiang and Mukherjee 1998)

$$\rho_{\gamma\ \mathrm{EGRET}} \sim \left(\frac{P_{\gamma0}}{P_B}\right)^{-\gamma_2} \Theta(P_{\gamma0} - P_B) + \qquad (12)$$
$$\left(\frac{P_{\gamma0}}{P_B}\right)^{-\gamma_1} \Theta(P_B - P_{\gamma0}) \quad ,$$

where $\gamma_1 \approx 1.2$, $\gamma_2 = 2.2\pm0.1$, $\log P_B \approx 14.9$ W Hz^{-1} sr^{-1} (corresponding to $L_B \approx 1.1\times10^{46}$ erg s^{-1}) and $\Theta(x)$ is a step function. $P_{\gamma0} = P_\gamma/f(z)$, where $f(z) = (1+z)^\beta$ with $\beta = 2.7\pm0.7$. Using equation (13), we can rewrite equation (9) as

$$n_{\mathrm{obs}} d(\log_{10}P_{\gamma\mathrm{f}}) = 4\pi\log_{\mathrm{e}}10 \left(\frac{2\mathrm{c}}{\mathrm{H}_0}\right)^3 \int_0^{\mathrm{z_{max}}} \qquad (13)$$
$$\frac{[(1+z)^{-1/2}-1]^2}{(1+z)^{5/2}} \rho_{\gamma\ \mathrm{EGRET}} P_{\gamma\mathrm{f}} dz\ d(\log_{10}P_{\gamma\mathrm{f}})$$

where the upper limit of the integral is min($z_{\max}$, 5). We calculated the γ-ray luminosity distribution using equation (14). In our calculation, we used the minimum value of the average γ-ray flux in our sample as the flux sensitivity, which is consistent with that used by Chiang and Mukherjee (1998), and $\beta = 2.2$. The maximum deviation is 0.12 for the expected γ-ray luminosity distribution calculated by equation (14). Therefore, the KS test indicates that the null hypothesis cannot be rejected at the $> 90\%$ confidence level. A comparison of the observed and expected cumulative γ-ray luminosity distributions is shown in the panel (C) of figure 2..

4. Conclusion and Discussion

Using γ-ray data of the blazars in the third EGRET catalog (Hartman et al. 1999) and radio data at 5 GHz, we used two methods to consider the correlation between the radio and γ-ray luminosities in the high and low states as well as in the average case. We first made a partial correlation analysis for the radio and γ-ray luminosities. Our results indicate that there are, at least marginal, correlations between the radio and γ-ray luminosities for the three cases. Second, we calculated the γ-ray luminosity distributions of the blazars by assuming a correlation between the radio and γ-ray luminosities (the correlation coefficients were determined by the observed data, see equations (6), (5) and (7) for both the low and high states as well as the average case) and using the γ-ray luminosity functions given by equation (12). We found that the expected γ-ray luminosity distributions are consistent with the observed data by using KS test (see figure 2.). Therefore, after using two statistical methods, we conclude that there is at least some correlation between the radio and γ-ray luminosities within a reasonable parameter range.

We also used the γ-ray luminosity functions given by Chiang and Mukherjee (1998) to estimate the γ-ray luminosity distribution. It should be noted that in their calculation of the γ-ray luminosity function, Chiang and Mukherjee (1998) used the 1 Jy radio catalog of Kühr et al. (1981) as an additional criterion to reduce the selection effects resulting from an incomplete redshift sample of AGNs. Therefore, there are 34 AGNs in their sample. The excluded blazars either fail to meet the significance limit, $(TS)^{1/2} = 4$, or the 1 Jy radio flux limit. In the calculation, they introduced a radio completeness function [see equation (7) of their paper] to reflect that the sample is restricted to being in the Kühr catalog. Therefore, although they did not explicitly assume a correlation between the radio and γ-ray luminosities, they did include an assumption that all blazars must be observed at the radio band and that their radio energy fluxes must be greater than 1 Jy. Obviously, this assumption is a key factor by which the expected gamma-ray luminosity distribution can roughly explain the observed data. In order to account for it, we note that Chiang et al. (1995) used the first EGRET catalog to obtain a gamma-ray luminosity function by modeling the optical evolution of their sources simultaneously with the gamma-ray evolution. The obtained γ-ray luminosity function is the same as equation (13) with different indexes ($\gamma_1 = 2.9$ and $\gamma_2 = 2.6$). When we used the result of Chiang et al. (1995) to estimate the gamma-ray luminosity distribution, the result was not consistent with the new EGRET catalog at all (see dot-dashed curve in the panel (C) of figure 2.).

From the KS test, we can see that the γ-ray luminosity distributions calculated by using equation (12) is better than that calculated by using equation (14). The former indicates a peak at $\log P_{\gamma \mathrm{f}} \sim 16.75$, which is consistent with the observed data. The later indicates a wider peak from $\log P_{\gamma \mathrm{f}} \sim 15$ to $\log P_{\gamma \mathrm{f}} \sim 17.5$. In figure 3., we show a comparison of the expected differential γ-ray luminosity distributions with the observed data. Further, we use the possible threshold of GLAST, $F_{\gamma\ \mathrm{lim}} \sim 3 \times 10^{-9}$ cm^{-2} s^{-1} (Kamae et al. 1999), to expect the γ-ray luminosity distributions using equations (12) and (14), respectively. The results are shown in figure 4.. Here, we have normalized the distributions to make the areas covered by the curves be the same. It can be seen that they have roughly the same shapes, but the former peaks are at $\log P_{\gamma \mathrm{f}} = 15.6$ and the later at $\log P_{\gamma \mathrm{f}} = 16.3$. We expect that this difference will be examined by GLAST.

From an observational point of view, there are some differences between BL Lacertae objects and flat spectral radio quasars (FSRQs), with the former showing no/weak emission lines, steeper X-ray spectra, and the later showing strong emission lines and flatter X-ray spectra. They are discussed separately in some cases (see Fossati et al. 1998; Ghisellini et al. 1998). But they both show a similar flat radio spectrum and a similar GeV γ-ray spectrum. Since we only considered the radio and the γ-ray regions, we discussed them both together.

Based on a statistical analysis, we have discussed the correlation between the γ-ray and the radio regions using the higher frequency radio data, the higher and lower states γ-ray and the radio regions (Fan et al. 1998; Cheng et al. 2000). We found that there is a closer correlation between the γ-ray emission and the high frequency (1.3 mm, 230 GHz) radio emission for the maximum data than between the γ-ray and the lower frequency (5GHz) radio emission (Fan et al. 1998). When we revisited the multiwavelength correlation using the compiled data, we found that there are very strong correlations between F_{X} and F_{O}, and F_{O} and F_{K} in both the low and high states. However, a strong correlation between F_{X} and F_{K} exists only in the low state. There are also hints of an anti-correlation between F_{γ} and F_{X} as well as $F_{rm\gamma}$ and F_{O}, and a positive correlation between F_{γ} and F_{R}. But the correlation between the γ-ray and the radio is not as strong as compared with those between F_{X} and F_{O}, and F_{O} and F_{K} (Cheng et al. 2000). Our present result is consistent with our previous ones. Besides, we wish to mention that there are 10 sources without any available redshift. There is no difference between the results obtained with those 10 sources both excluded and included.

Physically, if high-energy electrons in the jet are responsible for the radio and γ-ray emission, it would then be possible that radio photons are produced by the synchrotron radiation of these electrons, and that γ-rays are produced by the inverse Compton scattering of ambient lower energy photons, which may be the synchrotron photons. Therefore, there should exist a correlation between the radio and γ-ray luminosity to some extent. In fact, it is one of the predictions in the synchrotron self-Compton (SSC) models (e.g. Maraschi et al. 1992). Obviously, the seed photons may also be radiated directly from the accretion disk or disk photons scattered by a broad line region or wind material above the disk into the jet path (e.g. Dermer, Schlickeiser 1993; Sikora et al. 1994; Blandford, Levinson 1995; Zhang, Cheng 1997).

This work is partially supported by the Outstanding Researcher Awards of the University of Hong Kong, a Croucher Foundation Senior Research Fellowship and the National 973 projection of China (NKBRSF G19990754). This research has made use of data from the University of Michigan Radio Astronomy Observatory, which is supported by funds from the University of Michigan.

References

Blandford, R.D., Levinson, A. 1995, ApJ, 441, 79
Cheng, K.S., Ding, W.K.Y. 1994, A&A, 288, 97
Cheng, K.S., Yu, K.N.,& Ding, K.Y. 1993, A&A, 275, 53
Cheng, K.S., Zhang, X., & Zhang, L. 2000, ApJ, 537, 80
Chiang, J., Fichtel, C.E., von Montigny, C., Nolan, P.L. & Petrosian, V. 1995, ApJ, 452, 156
Chiang, J., & Mukherjee, R. 1998, ApJ, 496, 752
Dermer, C.D., & Schlickeiser, R. 1993, ApJ, 416, 458
Dermer, C.D., Schlickeiser R., & Mastichiadis A. 1992, A&A, 256, L27
Dondi, L., & Ghisellini, G. 1995, MNRAS, 273, 583
Dunlop, J.S., & Peacock, J.A. 1990, MNRAS, 247, 19
Fan, J.H., Adam, G., Xie, G.Z., Cao, S.L., Lin, R.G., & Copin, Y. 1998, A&A, 338, 27
Ghisellini, G., Padovani, P., Celotti, A., Maraschi, L. 1993, ApJ, 407, 65
Hartman, R.C. Bertsch, D.L., Bloom, S.D., Chen, A.W., Deines-Jones, P., Esposito, J.A., Fichtel, C.E., Friedlander, D.P., et al. 1999, ApJS, 123, 79
Kamae, T., Ohsugi, T., Thompson, D.J., Watanabe, K. 1999, astro-ph/9901187
Kühr, H., Witzel, A., Pauliny-Toth, I.I.K., Nauber, U. 1981, A&AS, 45, 367
Mannheim, K. 1993, A&A, 269, 67
Mannheim, K., & Biermann, P.L. 1992, A&A, 253, L21
Maraschi, L., Ghisellini, G., & Celotti, A. 1992, ApJ, 397, L5
Mattox, J.R., Schachter, J., Molnar, L., Hartman, R.C., & Patnaik, A.R. 1997, ApJ, 481, 95 Mücke, A., Pohl, M., Reich,P., Reich, W., Schlickeiser, R., Fichtel, C.E., Hartman, R.C., Kanbach, G., et al. 1997, A&A, 320, 33
Padovani, P. 1992, A&A, 256, 399
Padovani, P., Ghisellini, G., Fabian, A.C., & Celotti, A. 1993, MNRAS, 260, L21
Press, W., Flannery, B., Teukolsky, S., Vetterling, W. 1992, Numerical Recipes: The Art of Scientific Computing 2nd ed., (Cambridge Cambridge Univ. Press), p
Salamon, M.H. & Stecker, F.W. 1994, ApJ, 430, L21
Sikora, M., Begelman, M.C., & Rees, M.J. 1994, ApJ, 421, 153
Stecker, F.W., & Salmon, M.H. 1996, ApJ, 464, 600
Stecker, F.W., Salmon, M.H., & Malkan, M.A. 1993, ApJ, 410, L71
Xie, G.Z., Zhang, Y.H., & Fan, J.H. 1997, ApJ, 477, 114
Zhang, L., & Cheng, K.S. 1997, ApJ, 488, 94
Zhou, Y.Y., Lu, Y.J., Wang, T.G., Yu, K.N., Young, E.C.M. 1997, ApJ, 484, L47